

Vibrations of a weakly nondegenerate 1D-3D multi-structure

A. G. ASLANYAN¹⁾, J. DRONKA²⁾, G. MISHURIS²⁾, Ö. SELSIL³⁾

¹⁾*Druzhba St. 5, kv. 355, Khimki, Moscow Region
141400, Russia*

²⁾*Rzeszów University of Technology
Department of Mathematics
W. Pola 2, 35-959, Rzeszów, Poland*

³⁾*The University of Liverpool
Department of Mathematical Sciences
L69 7ZL, Liverpool, UK*

WE STUDY the effect of the transition between *degenerate* and *nondegenerate* configurations for a 1D-3D multi-structure, by considering a particular *nondegenerate configuration*. Analytical asymptotic formulae are derived for the first six eigenfrequencies which include information about the location of the 1D parts (legs) of the multi-structure. This enables us to analyse the transition region by moving the legs closer to each other. Accuracy of the asymptotic formulae is compared with numerical solution for the pile structure (skeleton) and with finite element computations. Some inaccuracies associated with numerical and finite element computations are discussed. In addition, a discussion on two-sided estimates for the eigenfrequencies is also included.

1. Introduction

THE ANALYSIS OF MULTI-STRUCTURES is still a fairly new subject. To clarify the terminology, we use the word multi-structure to mean a union of structures, for which the limit dimensions are different. These problems are classified as singularly perturbed, hence they are difficult to treat numerically due to the presence of a small parameter usually associated with the geometry (see MAZ'YA, NAZAROV and PLAMENEVSKII [1]). There are two major publications on the subject, namely the comprehensive monographs by CIARLET [2] and KOZLOV, MAZ'YA and MOVCHAN [3], in which the methods proposed to treat the stated problems differ fundamentally. The first adopts a variational approach, whereas the second employs the method of compound asymptotic expansions, based on the papers by KOZLOV, MAZ'YA and MOVCHAN [4–6].

In recent years, ASLANYAN, MOVCHAN and SELSIL published a number of papers on this topic, more precisely on eigenvalue problems posed for 2D-3D

and 1D-3D multi-structures [7–9]. The main emphasis of these papers was on the derivation of analytical asymptotic formulae for the first six eigenfrequencies of the above mentioned multi-structures (this could be used in a number of practical applications by engineers and other scientists as these structures do exist, for example, the Aquapark, Moscow and Charles de Gaulle Airport, Paris, which have both partly collapsed, and can be considered as multi-structures).

There are also very challenging mathematical issues of interest associated with problems of multi-structures, for example, two-sided estimates for the eigenfrequencies of these structures require rigorous mathematical analysis. We note that the representation of these estimates was given in KOZLOV, MAZ'YA and MOVCHAN [3], as well as the particular estimates for certain types of multi-structures (for *degenerate multi-structures* under certain restrictions related to the position of the 1D parts). The definition of the terminology *degenerate multi-structure* was given in KOZLOV, MAZ'YA and MOVCHAN [3] and will be discussed later in the present paper. For now, we can simply say that by the term *degenerate multi-structure* we mean that the determinant of the stiffness matrix associated with the pile structure (the skeleton of the multi-structure) (see ASPLUND [10]) is equal to zero. If this requirement is not satisfied, the term *nondegenerate multi-structure* will be used.

Following the definitions above, another matter of interest is to understand the existence of the nonzero determinant of the stiffness matrix being small (by small we mean a certain degree of the small parameter associated with the multi-structure). This paper is mainly concerned with these particular types of 1D-3D multi-structures, so-called *weakly nondegenerate multi-structures*. Here, we derive analytical asymptotic formulae for the first six eigenfrequencies of a particular example of a *weakly nondegenerate multi-structure*, and we discuss the transition between *degeneracy* and *nondegeneracy*. A specific example may appear to be far from a general analysis, but we note that general asymptotic formulae for the eigenfrequencies of a *weakly nondegenerate multi-structure* are impossible to construct as there is more than one type of *weakly nondegenerate 1D-3D multi-structure*. This idea will be discussed in more detail in the present paper. As in the previous papers, we also limit this analysis to the first six eigenfrequencies of the multi-structure since these eigenfrequencies correspond to rigid body motion of the 3D body, i.e. they are crucial for the safety of the multi-structure as they are the modes which require the most energy.

In Sec. 2 we summarize the main results, including the representations of the analytical asymptotic formulae for the first six eigenfrequencies of a particular *weakly nondegenerate 1D-3D multi-structure*. We formulate the eigenvalue problem associated with this multi-structure and introduce various notations used throughout the paper in Sec. 3. In addition, we present general asymptotics for the pile structure (the skeleton) associated with the multi-structure. This section

ends with a detailed discussion on the general definition of a *weakly nondegenerate 1D-3D multi-structure*. A particular example of this type of structure is given in Sec. 4., where we carry out a detailed analysis and compare our results with numerical solutions and finite element computations. An additional example is also included in this section to clarify the difference between two structures which, at first, may appear to be identical. Concluding remarks can be found in Sec. 5. Appendix A is related to the derivation of so-called lock forces and moments, i.e. the forces and moments exerted by the 1D parts of the multi-structure onto the 3D part. These 1D parts will be called “the legs”. Finally, Appendix B deals with an auxiliary lemma on the symmetry and positive definiteness of a certain matrix, crucial to our analysis.

2. Summary of main results

The main result of the present paper is the investigation of the effect of the transition between *degenerate* and *nondegenerate* configurations for a 1D-3D multi-structure.

The following analytical asymptotic formulae

$$f_k \sim \frac{1}{2\pi} \frac{b}{l} \sqrt{\frac{E l y_k}{\rho \Omega_0}}, \quad k = 1, 2, \quad f_k \sim \frac{1}{2\pi} \frac{b}{l} \sqrt{\frac{E l^2 y_k}{\rho \Omega_0 L}}, \quad k = 3, \dots, 6, \quad b \rightarrow 0,$$

which are constructed for the first six eigenfrequencies associated with the particular *nondegenerate* configuration of a 1D-3D multi-structure shown in Fig. 2, make it possible to analyse the behaviour of the solution with respect to all the parameters of the structure. Here, E is the Young’s modulus, ρ is the density, Ω_0 is the volume of the 3D body, y_k , $k = 1, 2, 3$, are the solutions of certain quadratic equations (see (4.6)–(4.8)), and l , L and b are the lengths and the diameter associated with the legs of the multi-structure. We note that Eqs. (4.6)–(4.8) and hence the analytical asymptotic formulae above, include information about the location of the legs of the multi-structure.

By considering different configurations of this particular *nondegenerate multi-structure*, more precisely, by moving the legs of the structure closer to each other, we analyse the transition to *degeneracy*. This transition region is carefully analysed and the accuracy of the asymptotic formulae is compared with the numerical solution for the pile structure using Matlab [11] and with the finite element solution for the 1D-3D multi-structure using COSMOS [12]. Here, we note that the numerical solution is consistent with the finite element calculations, even for small values of the distance between the legs of the structure. We also show that both of these solutions produce a certain degree of inaccuracy in the case when some of the eigenfrequencies are close to each other. This does not

happen with the asymptotic formulae, which is reliable in the regions where the inaccuracies occur. In addition, we observe an unexpected effect when the legs are close to the edges. In this case, the eigenfrequencies obtained from both the numerical solution (using Matlab) and the asymptotic formulae differ considerably from those obtained from the finite element solution (using COSMOS).

To establish two-sided estimates for the eigenfrequencies of the finite dimensional approximation to the 1D-3D multi-structure, it is important to know the value of the constant Q in

$$(2.1) \quad \frac{\rho\nu_k^2}{1 + Q\rho\nu_k^2} \leq \rho\omega_k^2 \leq \rho\nu_k^2,$$

where $\rho\omega^2$ is the spectral parameter of the eigenvalue problem (3.6)–(3.8) and $\rho\nu_k^2$ is the spectral parameter of the corresponding eigenvalue problem for the pile structure. However, it is difficult to determine this constant rigorously. In fact, it is only possible to estimate it in terms of the small parameter associated with the multi-structure. Our calculations lead to the result that the value for the constant Q is possibly different for *degenerate* and *nondegenerate 1D-3D multi-structures*.

3. General considerations for nondegenerate multi-structures

In this section, we first formulate an eigenvalue problem of three-dimensional linear elasticity, with reference to [3], describe the general asymptotics for the skeleton of the multi-structure and discuss the definition of *weak nondegeneracy*.

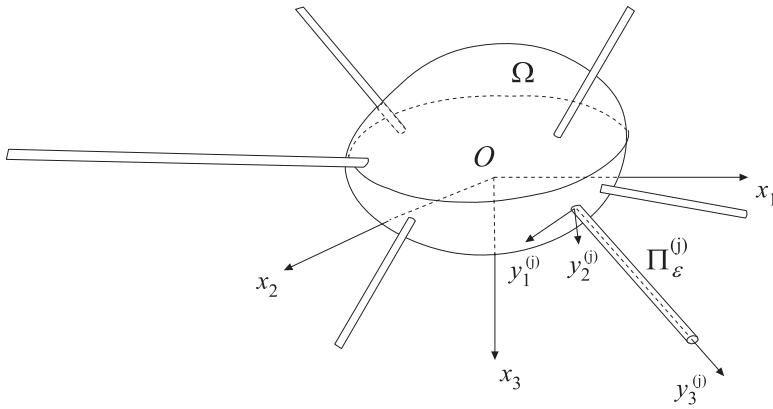
3.1. Problem formulation

Let $\mathbf{x} = (x_1, x_2, x_3)$ denote the Cartesian coordinates in \mathbb{R}^3 , and $(\mathbf{e}_1, \mathbf{e}_2, \mathbf{e}_3)$ denote the corresponding orthogonal basis of unit vectors. Now consider a bounded and convex domain in \mathbb{R}^3 , denoted by Ω , with Lipschitz boundary $\partial\Omega$, see Fig. 1. We use $\mathbf{a}^{(j)}$, $j = 1, 2, 3, \dots, K$ to denote K given points on $\partial\Omega$, at which K segments $r^{(j)}$ of length $l^{(j)}$ are connected to Ω . We formally define these segments as

$$(3.1) \quad r^{(j)} = \left\{ \mathbf{x} \in \mathbb{R}^3 : \mathbf{x} = \mathbf{a}^{(j)} + t\boldsymbol{\mu}^{(j)}, \quad 0 \leq t \leq l^{(j)} \right\}, \quad j = 1, 2, 3, \dots, K.$$

Here, $\boldsymbol{\mu}^{(j)}$ are given unit vectors satisfying the condition $\mathbf{n} \cdot \boldsymbol{\mu}^{(j)} > 0$, where \mathbf{n} is the unit outward normal to $\partial\Omega$ at the point $\mathbf{a}^{(j)}$, and $\mathbf{b}^{(j)} = \mathbf{a}^{(j)} + l^{(j)}\boldsymbol{\mu}^{(j)}$ are the opposite ends of the segments $r^{(j)}$. Without loss of generality, we assume that the center of mass is situated along the Ox_3 -axis (directed downwards), i.e.

$$\int_{\Omega} x_k \, d\mathbf{x} = 0, \quad k = 1, 2.$$

FIG. 1. 1D-3D homogeneous multi-structure Ω_ε .

Next, we introduce the local Cartesian coordinate systems $\mathbf{y}^{(j)} = (y_1^{(j)}, y_2^{(j)}, y_3^{(j)})$ along each segment $r^{(j)}$, the new origin being at the point $\mathbf{a}^{(j)}$ for each segment and the $y_3^{(j)}$ -axis being directed along the vector $\boldsymbol{\mu}^{(j)}$. We connect the local coordinate systems $\mathbf{y}^{(j)}$ with \mathbf{x} in the following way:

$$(3.2) \quad \mathbf{x} = \mathbf{a}^{(j)} + \mathbf{\Lambda}^{(j)} \mathbf{y}^{(j)},$$

where $\mathbf{\Lambda}^{(j)}$ is an orthogonal matrix and

$$(3.3) \quad \boldsymbol{\mu}^{(j)} = \mathbf{\Lambda}^{(j)} \mathbf{e}_3.$$

We note that the rotation of the local coordinate system on the $y_1^{(j)} y_2^{(j)}$ -plane can be chosen arbitrarily.

Below, each segment $r^{(j)}$ is considered as the axis of a thin cylinder

$$\Pi_\varepsilon^{(j)} = \left\{ \mathbf{y}^{(j)} : 0 < y_3^{(j)} < l^{(j)}, \varepsilon^{-1}(y_1^{(j)}, y_2^{(j)}) \in g^{(j)} \subset \mathbb{R}^2 \right\},$$

where $g^{(j)}$ is a bounded domain with Lipschitz boundary and ε is a small dimensionless parameter which denotes the maximum characteristic ratio of the diameter of a leg to its length.

We also use the notation $S_\varepsilon^{(j)}$ for the base regions of the thin cylinders $\Pi_\varepsilon^{(j)}$ which contain the points $\mathbf{b}^{(j)}$ and let

$$(3.4) \quad S_\varepsilon = \cup_{j=1}^K S_\varepsilon^{(j)}.$$

Now, we can define the 1D-3D multi-structure as

$$(3.5) \quad \bar{\Omega}_\varepsilon = \bar{\Omega} \cup \bar{\Pi}_\varepsilon^{(1)} \cup \dots \cup \bar{\Pi}_\varepsilon^{(K)},$$

and we consider the following eigenvalue problem:

$$(3.6) \quad -\mathbf{L}\mathbf{u} = \rho\omega^2\mathbf{u}, \quad \mathbf{x} \in \Omega \cup_{j=1}^K \Pi_\varepsilon^{(j)},$$

$$(3.7) \quad \boldsymbol{\sigma}^{(n)}(\mathbf{u}) = \mathbf{0}, \quad \mathbf{x} \in \partial\Omega_\varepsilon \setminus S_\varepsilon,$$

$$(3.8) \quad \mathbf{u} = \mathbf{0}, \quad \mathbf{x} \in S_\varepsilon,$$

where

$$\mathbf{L} = \mu\nabla^2 + (\lambda + \mu) \text{grad div}$$

is the Lamé operator, \mathbf{u} is the displacement vector, $\boldsymbol{\sigma}^{(n)}(\mathbf{u}) = \boldsymbol{\sigma}\mathbf{n}$ is the stress vector, ρ is the mass density and ω is the corresponding eigenfrequency. Here, λ and μ are the Lamé elastic moduli.

As shown in [3] (p. 251, Theorem 6.1), the following estimate holds true for the spectral parameter $\rho\omega^2$ of the problem (3.6)–(3.8):

$$\frac{\rho\nu_k^2}{1 + \mathcal{Q}\rho\nu_k^2} \leq \rho\omega_k^2 \leq \rho\nu_k^2, \quad k = 1, \dots, 6,$$

where (see [3], p. 251, Eq. (6.1.8))

$$(3.9) \quad \rho\nu_k^2 = \min_{\mathbf{v} \neq \mathbf{0}} \frac{a(\mathbf{v}, \mathbf{v})}{(\mathbf{v}, \mathbf{v})}$$

is the spectral parameter for the corresponding eigenvalue problem for the pile structure (the skeleton of the multi-structure). In Eq. (3.9), $a(\cdot, \cdot)$ is the bilinear form associated with the Lamé operator and \mathbf{v} belongs to the respective subspace of the possible pile structure motion (rigid body translations and rotations).

The value of the parameter \mathcal{Q} in (2.1) depends on the geometry and the material properties of the multi-structure, and in general, it is a difficult task to find its value. In [3], the analysis was done for a specific *degenerate multi-structure*, for which

$$(3.10) \quad \mathcal{Q} = O(\varepsilon^{-2}), \quad \varepsilon \rightarrow 0.$$

3.2. Description of the general asymptotics for the skeleton of the multi-structure

We assume that the 3D body Ω moves like a rigid body, i.e.

$$(3.11) \quad \mathbf{v} = \boldsymbol{\alpha} + \boldsymbol{\beta} \times \mathbf{x}, \quad \text{in } \Omega,$$

where $\boldsymbol{\alpha}$ and $\boldsymbol{\beta}$ are constant vectors. We also assume that the displacements in (3.11) are valid under the effect of the body forces given by

$$(3.12) \quad \boldsymbol{\Psi} = \mathbf{c} + \mathbf{d} \times \mathbf{x},$$

where \mathbf{c} and \mathbf{d} are constant vectors. Here, it is important to note that the vectors \mathbf{v} and Ψ are not independent of each other, i.e.

$$(3.13) \quad \Psi = \Psi(\mathbf{v}) \quad \text{or} \quad \mathbf{v} = \mathbf{v}(\Psi).$$

Now we obtain this dependence explicitly.

Let us characterise the interaction between the 3D body Ω and the elastic legs $\Pi_\varepsilon^{(j)}$, $j = 1, \dots, K$ by concentrated forces $\mathcal{F}^{(j)}$ and concentrated moments $\mathcal{M}^{(j)}$ applied at the junction points $\mathbf{a}^{(j)}$. The resultant force \mathcal{F} and the resultant moment \mathcal{M} , caused by the body forces (3.12), are applied to the body Ω . Hence, the equilibrium equations have the form

$$(3.14) \quad \mathcal{F} + \sum_{j=1}^K \mathcal{F}^{(j)} = \mathbf{0}, \quad \mathcal{M} + \sum_{j=1}^K (\mathcal{M}^{(j)} + \mathbf{a}^{(j)} \times \mathcal{F}^{(j)}) = \mathbf{0}.$$

We refer to monograph [3] (p. 177), which is outlined in Appendix A, for the forces and moments at junction points $\mathbf{a}^{(j)}$, exerted by the elastic legs onto the 3D body Ω and we use the following relation to establish the link between global and local coordinates:

$$(3.15) \quad \hat{\mathbf{w}}^{(j)} = \mathbf{\Lambda}^{(j)} \mathbf{w}.$$

Hence, the forces and moments can be written in global coordinates as

$$(3.16) \quad \mathcal{F}^{(j)} = -(\mathbf{\Lambda}^{(j)})^* \mathbf{R}^{(j)} \mathbf{\Lambda}^{(j)} (\boldsymbol{\alpha} + \boldsymbol{\beta} \times \mathbf{a}^{(j)}) - (\mathbf{\Lambda}^{(j)})^* \mathbf{Q}^{(j)} \mathbf{\Lambda}^{(j)} \boldsymbol{\beta},$$

$$(3.17) \quad \mathcal{M}^{(j)} = -(\mathbf{\Lambda}^{(j)})^* (\mathbf{Q}^{(j)})^\top \mathbf{\Lambda}^{(j)} (\boldsymbol{\alpha} + \boldsymbol{\beta} \times \mathbf{a}^{(j)}) - (\mathbf{\Lambda}^{(j)})^* \mathbf{T}^{(j)} \mathbf{\Lambda}^{(j)} \boldsymbol{\beta},$$

where

$$(3.18) \quad \mathbf{R}^{(j)} = \text{diag}\{12C_1^{(j)}/l^{(j)3}, 12C_2^{(j)}/l^{(j)3}, C_3^{(j)}/l^{(j)}\},$$

$$(3.19) \quad \mathbf{T}^{(j)} = \text{diag}\{4C_2^{(j)}/l^{(j)}, 4C_1^{(j)}/l^{(j)}, C_4^{(j)}/l^{(j)}\},$$

and

$$(3.20) \quad \mathbf{Q}^{(j)} = (6/l^{(j)2}) \begin{pmatrix} 0 & C_1^{(j)} & 0 \\ -C_2^{(j)} & 0 & 0 \\ 0 & 0 & 0 \end{pmatrix}.$$

Here, $(\mathbf{\Lambda}^{(j)})^*$ denotes the adjoint matrix of $\mathbf{\Lambda}^{(j)}$. The parameters $C_i^{(j)}$, $i = 1, 2, 3, 4, j = 1, \dots, K$ are known as the stiffness coefficients associated with

the legs $\Pi_i^{(j)}$ and their definitions are also given in Appendix A. We also used the following

$$\hat{\boldsymbol{\beta}}^{(j)} \times \hat{\mathbf{a}}^{(j)} = \boldsymbol{\Lambda}^{(j)}(\boldsymbol{\beta} \times \mathbf{a}^{(j)}),$$

which is a simple consequence of (3.15).

If we consider a matrix

$$(3.21) \quad \mathbf{A}^{(j)} = \begin{pmatrix} 0 & -a_3^{(j)} & a_2^{(j)} \\ a_3^{(j)} & 0 & -a_1^{(j)} \\ -a_2^{(j)} & a_1^{(j)} & 0 \end{pmatrix},$$

it is clear that we can write

$$(3.22) \quad \mathbf{a}^{(j)} \times \mathbf{b} = \mathbf{A}^{(j)}\mathbf{b},$$

where \mathbf{b} is an arbitrary vector.

Now, using (3.22) and (3.16)–(3.20), the equilibrium equations (3.14) take the form

$$(3.23) \quad \mathcal{F} = \Phi_{1,1}\boldsymbol{\alpha} + \Phi_{1,2}\boldsymbol{\beta}, \quad \mathcal{M} = \Phi_{2,1}\boldsymbol{\alpha} + \Phi_{2,2}\boldsymbol{\beta},$$

where $\Phi_{k,l}$, $k, l = 1, 2$ are 3×3 matrices:

$$(3.24) \quad \Phi_{1,1} = \sum_{j=1}^K (\boldsymbol{\Lambda}^{(j)})^* \mathbf{R}^{(j)} \boldsymbol{\Lambda}^{(j)},$$

$$(3.25) \quad \Phi_{1,2} = \sum_{j=1}^K \left\{ (\boldsymbol{\Lambda}^{(j)})^* \mathbf{Q}^{(j)} \boldsymbol{\Lambda}^{(j)} - (\boldsymbol{\Lambda}^{(j)})^* \mathbf{R}^{(j)} \boldsymbol{\Lambda}^{(j)} \mathbf{A}^{(j)} \right\},$$

$$(3.26) \quad \Phi_{2,1} = \sum_{j=1}^K \left\{ (\boldsymbol{\Lambda}^{(j)})^* (\mathbf{Q}^{(j)})^\top \boldsymbol{\Lambda}^{(j)} + \mathbf{A}^{(j)} (\boldsymbol{\Lambda}^{(j)})^* \mathbf{R}^{(j)} \boldsymbol{\Lambda}^{(j)} \right\},$$

$$(3.27) \quad \Phi_{2,2} = \sum_{j=1}^K \left\{ (\boldsymbol{\Lambda}^{(j)})^* \mathbf{T}^{(j)} \boldsymbol{\Lambda}^{(j)} - (\boldsymbol{\Lambda}^{(j)})^* (\mathbf{Q}^{(j)})^\top \boldsymbol{\Lambda}^{(j)} \mathbf{A}^{(j)} \right\} \\ + \sum_{j=1}^K \left\{ \mathbf{A}^{(j)} (\boldsymbol{\Lambda}^{(j)})^* \mathbf{Q}^{(j)} \boldsymbol{\Lambda}^{(j)} - \mathbf{A}^{(j)} (\boldsymbol{\Lambda}^{(j)})^* \mathbf{R}^{(j)} \boldsymbol{\Lambda}^{(j)} \mathbf{A}^{(j)} \right\}.$$

Hence, we define by Φ a 6×6 matrix such that

$$(3.28) \quad \Phi = \begin{pmatrix} \Phi_{1,1} & \Phi_{1,2} \\ \Phi_{2,1} & \Phi_{2,2} \end{pmatrix},$$

which is symmetric and positive definite (for the proof see Appendix B).

Next, we define a 6×6 matrix Γ as

$$(3.29) \quad \Gamma = \begin{pmatrix} \Gamma_1 & \Gamma_2 \\ \Gamma_3 & \Gamma_4 \end{pmatrix},$$

where

$$\Gamma_1 = \text{diag}\{\Omega_0, \Omega_0, \Omega_0\},$$

$$(3.30) \quad \Gamma_2 = \Gamma_3^\top = \begin{pmatrix} 0 & K_0 & 0 \\ -K_0 & 0 & 0 \\ 0 & 0 & 0 \end{pmatrix}, \quad \Gamma_4 = \begin{pmatrix} I_1 & -R_{1,2} & -R_{1,3} \\ -R_{1,2} & I_2 & -R_{2,3} \\ -R_{1,3} & -R_{2,3} & I_3 \end{pmatrix},$$

with

$$(3.31) \quad \begin{aligned} \Omega_0 &= \int_{\Omega} d\mathbf{x}, & K_0 &= \int_{\Omega} x_3 d\mathbf{x}, \\ I_k &= \int_{\Omega} (|\mathbf{x}|^2 - x_k^2) d\mathbf{x}, & k &= 1, 2, 3, \\ R_{k,l} &= \int_{\Omega} x_k x_l d\mathbf{x}, & k, l &= 1, 2, 3; k \neq l. \end{aligned}$$

As in [8], we have (see (3.12))

$$(3.32) \quad \mathcal{F} = \Gamma_1 \mathbf{c} + \Gamma_2 \mathbf{d}, \quad \mathcal{M} = \Gamma_3 \mathbf{c} + \Gamma_4 \mathbf{d}.$$

For the proof of symmetry and positive definiteness of the matrix Γ we again refer to [8]. Hence, we have

$$(3.33) \quad \Gamma = \Gamma^\top, \quad \Gamma > 0.$$

Now, defining two vectors

$$(3.34) \quad \boldsymbol{\eta} = (c_1, c_2, c_3, d_1, d_2, d_3)^\top,$$

and

$$(3.35) \quad \boldsymbol{\theta} = (\alpha_1, \alpha_2, \alpha_3, \beta_1, \beta_2, \beta_3)^\top,$$

we can rewrite the equilibrium equations for the multi-structure Ω_ε as (see (3.23) and (3.32))

$$(3.36) \quad \boldsymbol{\Phi}\boldsymbol{\theta} = \boldsymbol{\Gamma}\boldsymbol{\eta},$$

which establishes (3.13).

Finally, we use formula (3.9) to derive

$$(3.37) \quad t \equiv \rho\nu^2 = \min_{\mathbf{v} \neq \mathbf{0}} \frac{\int_{\Omega} (\mathbf{v}, \boldsymbol{\Psi}(\mathbf{v})) d\mathbf{x}}{\int_{\Omega} (\mathbf{v}, \mathbf{v}) d\mathbf{x}},$$

where we also take the well-known D'Alembert's principle into account.

Lemma 1. *The characteristic equation for the auxiliary variational problem (3.37) has the following form:*

$$(3.38) \quad \det(\boldsymbol{\Phi} - t\boldsymbol{\Gamma}) = 0.$$

P r o o f. The displacements of the 3D body Ω up to the leading order can be written as (see (3.11))

$$(3.39) \quad \mathbf{v} = \mathbf{M}_1\boldsymbol{\theta},$$

where

$$(3.40) \quad \mathbf{M}_1(\mathbf{x}) = \begin{pmatrix} 1 & 0 & 0 & 0 & x_3 & -x_2 \\ 0 & 1 & 0 & -x_3 & 0 & x_1 \\ 0 & 0 & 1 & x_2 & -x_1 & 0 \end{pmatrix}.$$

Using equation (3.36) we also have

$$(3.41) \quad \boldsymbol{\Psi} = \mathbf{M}_1\boldsymbol{\eta} = \mathbf{M}_1\boldsymbol{\Gamma}^{-1}\boldsymbol{\Phi}\boldsymbol{\theta}.$$

Hence, by (3.37) and (3.39)–(3.41) we obtain

$$(3.42) \quad t = \min_{\boldsymbol{\theta} \neq \mathbf{0}} \frac{\int_{\Omega} (\mathbf{M}_0\boldsymbol{\theta}, \boldsymbol{\Gamma}^{-1}\boldsymbol{\Phi}\boldsymbol{\theta}) d\mathbf{x}}{\int_{\Omega} (\mathbf{M}_0\boldsymbol{\theta}, \boldsymbol{\theta}) d\mathbf{x}},$$

where $\mathbf{M}_0(\mathbf{x}) = \mathbf{M}_1^\top(\mathbf{x})\mathbf{M}_1(\mathbf{x})$. Here, we have also used the fact that $(\mathbf{N}_1\boldsymbol{\theta}, \mathbf{N}_2\boldsymbol{\theta}) = (\boldsymbol{\theta}, \mathbf{N}_1^\top\mathbf{N}_2\boldsymbol{\theta})$, for arbitrary matrices with the same dimension as \mathbf{M}_1 .

Since the matrix \mathbf{M}_0 in (3.42) is the only matrix which depends on \mathbf{x} , we obtain

$$(3.43) \quad t = \min_{\boldsymbol{\theta} \neq \mathbf{0}} \frac{(\boldsymbol{\theta}, \boldsymbol{\Phi}\boldsymbol{\theta})}{(\boldsymbol{\theta}, \boldsymbol{\Gamma}\boldsymbol{\theta})}.$$

Note that here we have also taken into account that

$$(3.44) \quad \int_{\Omega} \mathbf{M}_0(\mathbf{x})d\mathbf{x} = \boldsymbol{\Gamma}.$$

Hence, the proof is complete. \square

Since the matrices $\boldsymbol{\Phi}$ and $\boldsymbol{\Gamma}$ are symmetric and positive definite, all the roots of the equation (3.38) coincide with the eigenvalues of the positive definite matrix $\boldsymbol{\Phi}\boldsymbol{\Gamma}^{-1}$. Hence, they are all positive:

$$(3.45) \quad 0 < t_1 \leq t_2 \leq \dots \leq t_6.$$

Therefore, using (3.37), we obtain the following approximate values for the first six eigenfrequencies of the multi-structure Ω_ε :

$$(3.46) \quad f_k = \frac{1}{2\pi} \sqrt{t_k/\rho}, \quad k = 1, \dots, 6.$$

3.3. Definition of a weakly nondegenerate multi-structure

We remark that the eigenvalues t_k , $k = 1, \dots, 6$ (consequently f_k , $k = 1, \dots, 6$) are functions of the small parameter ε . In this section we clarify this dependence.

From formulae (3.29)–(3.31) it is apparent that the matrix $\boldsymbol{\Gamma}$ is not associated with the small parameter ε and gives information only about the 3D body Ω . On the other hand, the matrix $\boldsymbol{\Phi}$ is clearly a function of ε . The relevant description of the stiffness coefficients in (3.18)–(3.20) can be found in Appendix A (see (A.1)–(A.4)). It immediately follows that

$$(3.47) \quad \mathbf{R}^{(j)} = \varepsilon^2\mathbf{R}_0^{(j)} + \varepsilon^4\mathbf{R}_1^{(j)}, \quad \mathbf{T}^{(j)} = \varepsilon^4\mathbf{T}_1^{(j)}, \quad \mathbf{Q}^{(j)} = \varepsilon^4\mathbf{Q}_1^{(j)},$$

where

$$\begin{aligned}
\mathbf{R}_0^{(j)} &= \text{diag} \left\{ 0, 0, C_{3,0}^{(j)}/l^{(j)} \right\}, \\
\mathbf{R}_1^{(j)} &= \text{diag} \left\{ 12C_{1,0}^{(j)}/l^{(j)3}, 12C_2^{(j)}/l^{(j)3}, 0 \right\}, \\
(3.48) \quad \mathbf{T}_1^{(j)} &= \text{diag} \left\{ 4C_{2,0}^{(j)}/l^{(j)}, 4C_{1,0}^{(j)}/l^{(j)}, C_{4,0}^{(j)}/l^{(j)} \right\}, \\
\mathbf{Q}_1^{(j)} &= \frac{6}{l^{(j)2}} \begin{pmatrix} 0 & C_{1,0}^{(j)} & 0 \\ -C_{2,0}^{(j)} & 0 & 0 \\ 0 & 0 & 0 \end{pmatrix},
\end{aligned}$$

do not depend on the small parameter ε .

Consequently, formula (3.28) can be represented as

$$(3.49) \quad \mathbf{\Phi} = \varepsilon^2 \mathbf{\Phi}_0 + \varepsilon^4 \mathbf{\Phi}_1,$$

and therefore, equation (3.38) can be rewritten as

$$(3.50) \quad \det(\mathbf{\Phi}_0 + \varepsilon^2 \mathbf{\Phi}_1 - q\mathbf{\Gamma}) = 0,$$

where $q(\varepsilon) = t(\varepsilon)/\varepsilon^2$.

We note that if the matrix $\mathbf{\Phi}_0$ is nonsingular, then we can seek $q^{(k)}(\varepsilon)$ in the form

$$(3.51) \quad q^{(k)}(\varepsilon) = q_0^{(k)} + \varepsilon^2 q_1^{(k)} + O(\varepsilon^4), \quad \varepsilon \rightarrow 0, \quad k = 1, \dots, 6,$$

and to obtain $q_0^{(k)}$, we need to solve

$$(3.52) \quad \det(\mathbf{\Phi}_0 - q_0\mathbf{\Gamma}) = 0.$$

In [3], the definition of a *nondegenerate multi-structure* is given as follows: If the equalities

$$\boldsymbol{\mu}^{(j)} \cdot (\boldsymbol{\alpha} - \mathbf{a}^{(j)} \times \boldsymbol{\beta}) = 0, \quad j = 1, \dots, K,$$

imply that the vectors $\boldsymbol{\alpha}$ and $\boldsymbol{\beta}$ are zero, then the corresponding multi-structure is *nondegenerate*. This definition is equivalent to the requirement that the matrix $\mathbf{\Phi}_0$ should be nonsingular (and, of course, positive definite (see Appendix B)). Otherwise, the multi-structure is called *degenerate*.

However, despite the fact that $\mathbf{\Phi}_0$ does not depend on ε , it is possible to consider structures for which $\det(\mathbf{\Phi}_0)$ is comparable with some order of the small parameter ε , which is defined by the geometry of the legs. In what follows,

such structures are called *weakly nondegenerate*, for which formula (3.51) may not be applicable.

It is clear from this definition that there can be numerous configurations which would lead to *weakly nondegenerate* structures. In the next section, we investigate, in detail, a particular 1D-3D *weakly nondegenerate multi-structure* to illustrate this interesting effect.

4. Weakly nondegenerate multi-structures

4.1. A particular example: A 1D-3D multi-structure with six legs

In this section we study a particular configuration of a 1D-3D multi-structure, which leads to a certain degeneracy in the limit case, as shown in Fig. 2. As discussed in the previous sections, we would like to analyse the eigenfrequencies of this multi-structure, when the legs on each face move closer together. For simplicity, the 3D body is chosen as a parallelepiped of dimensions a_1, a_2, a_3 . The choice of the coordinate axes $Ox_1x_2x_3$ is also shown in Fig. 2. As mentioned in Sec. 3.1., the local $y_3^{(j)}$ -axes ($j = 1, \dots, 6$) are directed along the segments.

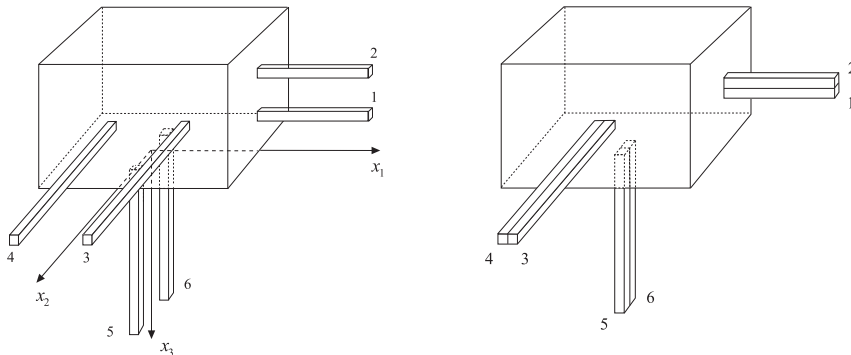


FIG. 2. A 1D-3D homogeneous multi-structure, illustrating the transition between *nondegeneracy* and *degeneracy*.

We assume that the legs are homogeneous with density ρ and isotropic with Young's modulus E and Poisson's ratio ν . We also assume that they have $b \times b$ cross-sections and lengths

$$l^{(1)} = l^{(2)} = l, \quad l^{(3)} = l^{(4)} = l^{(5)} = l^{(6)} = L.$$

Assuming that $l \leq L$, we introduce the dimensionless small parameter ε as b/l , which is the maximum characteristic ratio.

We use the following coordinates for the junction points:

$$(4.1) \quad \begin{aligned} \mathbf{a}^{(1)} &= (a_1/2, 0, -a_3/2 + p_3)^\top, & \mathbf{a}^{(2)} &= (a_1/2, 0, -a_3/2 - q_3)^\top, \\ \mathbf{a}^{(3)} &= (p_1, a_2/2, -a_3/2)^\top, & \mathbf{a}^{(4)} &= (-q_1, a_2/2, -a_3/2)^\top \\ \mathbf{a}^{(5)} &= (0, p_2, 0)^\top, & \mathbf{a}^{(6)} &= (0, -q_2, 0)^\top, \end{aligned}$$

where

$$(4.2) \quad 0 < p_k, q_k < a_k/2, \quad k = 1, 2, 3.$$

From Fig. 2 it is clear that the unit vectors defining the directions of the legs are

$$\boldsymbol{\mu}^{(1)} = \boldsymbol{\mu}^{(2)} = (1, 0, 0)^\top, \quad \boldsymbol{\mu}^{(3)} = \boldsymbol{\mu}^{(4)} = (0, 1, 0)^\top, \quad \boldsymbol{\mu}^{(5)} = \boldsymbol{\mu}^{(6)} = (0, 0, 1)^\top.$$

Hence, the transformation matrices are given as

$$\boldsymbol{\Lambda}^{(1)} = \boldsymbol{\Lambda}^{(2)} = \begin{pmatrix} 0 & 1 & 0 \\ 0 & 0 & 1 \\ 1 & 0 & 0 \end{pmatrix}, \quad \boldsymbol{\Lambda}^{(3)} = \boldsymbol{\Lambda}^{(4)} = \begin{pmatrix} 0 & 0 & 1 \\ 1 & 0 & 0 \\ 0 & 1 & 0 \end{pmatrix}, \quad \boldsymbol{\Lambda}^{(5)} = \boldsymbol{\Lambda}^{(6)} = \begin{pmatrix} 1 & 0 & 0 \\ 0 & 1 & 0 \\ 0 & 0 & 1 \end{pmatrix}.$$

Now, we construct the matrix $\boldsymbol{\Phi}_0$ (see (3.49)). The nonzero elements of the matrix $\boldsymbol{\Phi}_0$ are given as

$$(4.3) \quad \boldsymbol{\Phi}_0 = \left(\phi_{k,m}^{(0)} \right)_{k,m=1}^6,$$

$$(4.4) \quad \begin{aligned} \phi_{1,1}^{(0)} &= 2s_1, & \phi_{1,5}^{(0)} &= \phi_{5,1}^{(0)} = (p_3 - a_3 - q_3)s_1, \\ \phi_{2,2}^{(0)} &= \phi_{3,3}^{(0)} = 2s_2, & \phi_{2,4}^{(0)} &= \phi_{4,2}^{(0)} = a_3s_2, \\ \phi_{2,6}^{(0)} &= \phi_{6,2}^{(0)} = (p_1 - q_1)s_2, & \phi_{3,4}^{(0)} &= \phi_{4,3}^{(0)} = (p_2 - q_2)s_2, \\ \phi_{4,4}^{(0)} &= \left(\frac{a_3^2}{2} + p_2^2 + q_2^2 \right) s_2, & \phi_{4,6}^{(0)} &= \phi_{6,4}^{(0)} = \frac{a_3}{2} (p_1 - q_1) s_2, \\ \phi_{5,5}^{(0)} &= \left[\left(\frac{a_3}{2} - p_3 \right)^2 + \left(\frac{a_3}{2} + q_3 \right)^2 \right] s_1, & \phi_{6,6}^{(0)} &= (p_1^2 + q_1^2)s_2, \end{aligned}$$

where $s_1 = lE$ and $s_2 = l^2E/L$. We note that the matrix $\boldsymbol{\Phi}_0$ is nonsingular due to (4.2), which enables us to use representation (3.51). However, if p_k, q_k have smaller values, (3.51) may be violated and therefore, the matrix $\boldsymbol{\Phi}_1$ should

be taken into account in order to estimate the leading term of the asymptotic approximation accurately.

In addition, the components of the matrix $\mathbf{\Gamma}$ can be computed as (see (3.29)–(3.31))

$$(4.5) \quad \begin{aligned} \Omega_0 &= a_1 a_2 a_3, & K_0 &= -\frac{a_3}{2} \Omega_0, & I_1 &= \frac{1}{12} (a_2^2 + 4a_3^2) \Omega_0, \\ I_2 &= \frac{1}{12} (a_1^2 + 4a_3^2) \Omega_0, & I_3 &= \frac{1}{12} (a_1^2 + a_2^2) \Omega_0, \\ R_{k,l} &= 0, & k, l &= 1, 2, 3; & k &\neq l. \end{aligned}$$

After some manipulation, Eq. (3.52) can be split into three quadratic equations:

$$(4.6) \quad \frac{1}{12} (a_1^2 + a_3^2) y^2 - \left[p_3^2 + q_3^2 + \frac{1}{6} (a_1^2 + a_3^2) \right] y + (p_3 + q_3)^2 = 0,$$

where $y = \Omega_0 q_0 / s_1$, and

$$(4.7) \quad \frac{1}{12} (a_1^2 + a_2^2) y^2 - \left[p_1^2 + q_1^2 + \frac{1}{6} (a_1^2 + a_2^2) \right] y + (p_1 + q_1)^2 = 0,$$

$$(4.8) \quad \frac{1}{12} (a_2^2 + a_3^2) y^2 - \left[p_2^2 + q_2^2 + \frac{1}{6} (a_2^2 + a_3^2) \right] y + (p_2 + q_2)^2 = 0,$$

with $y = \Omega_0 q_0 / s_2$. This leads us to the following estimates for the first six eigenfrequencies:

$$(4.9) \quad \begin{aligned} f_k &\sim \frac{1}{2\pi} \frac{b}{l} \sqrt{\frac{E l y_k}{\rho \Omega_0}}, & k &= 1, 2, \\ f_k &\sim \frac{1}{2\pi} \frac{b}{l} \sqrt{\frac{E l^2 y_k}{\rho \Omega_0 L}}, & k &= 3, \dots, 6, & b &\rightarrow 0. \end{aligned}$$

We now consider the following numerical values:

$$(4.10) \quad \begin{aligned} a_1 &= a_2 = 108 \text{ [cm]}, & a_3 &= 60 \text{ [cm]}, & b &= 4 \text{ [cm]}, & l &= L = 200 \text{ [cm]}, \\ p_1 &= p_2 = q_1 = q_2 = (2 + 2p) \text{ [cm]}, & p_3 &= q_3 = (2 + p) \text{ [cm]}, \\ E &= 2.1 \cdot 10^{12} \text{ [g/(cm sec}^2\text{)]}, & \rho &= 7.8 \text{ [g/cm}^3\text{]}, & \nu &= 0.28. \end{aligned}$$

We note that the parameter p above is introduced to investigate the transition between *nondegeneracy* and *degeneracy*. More precisely, by changing p from 0 to 24 in the above configuration, we are moving the legs further apart.

To verify the accuracy of the asymptotic formulae (4.9), we solve equation (3.38) numerically, using Matlab (see Fig. 3). Further, we adopt the notations $f_r^{(j)}$, $f_t^{(j)}$, $j = 1, 2, 3$ (instead of f_k , $k = 1, \dots, 6$) for eigenfrequencies corresponding to rotations/translations about/along the x_j -axis, that is, the respective eigenvector $\boldsymbol{\theta} = (\alpha_1, \alpha_2, \alpha_3, \beta_1, \beta_2, \beta_3)^\top$ contains a dominating component associated with the type of motion. We note that $\boldsymbol{\theta} = \boldsymbol{\theta}(p)$ and the notations introduced above are accurate for small values of the parameter p (in our case $p < 15$). For larger values of p , we observe that some of the modes are a combination of two dominating components. However, we still adopt the same notations for all the values of the parameter p to avoid confusion.

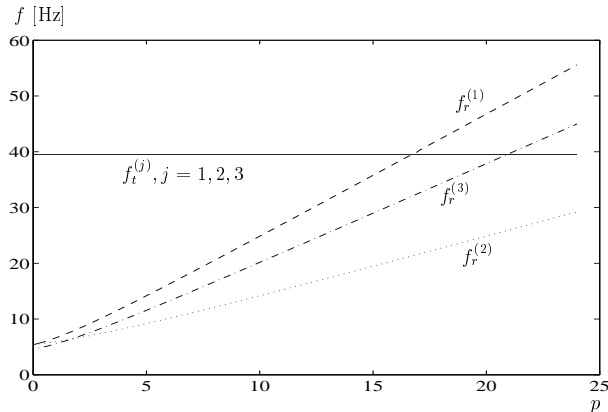


FIG. 3. Eigenfrequencies $f_r^{(j)}$ and $f_t^{(j)}$ versus the parameter p , where $j = 1, 2, 3$ indicate the respective rotation/translation about/along the x_j -axis.

At this point, we would like to mention that it is clear that the eigenfrequencies $f_t^{(j)}$, $j = 1, 2, 3$ are not significantly distinguishable, (see Fig. 3). More precisely, the difference between, for example, $f_t^{(1)}$ and $f_t^{(3)}$ is approximately $10^{-4}\%$.

We now compare these results with the asymptotic formulae (4.9). The results for the eigenfrequencies corresponding to rotation modes are presented in Fig. 4. In each graph, the solid line corresponds to the numerical solution of equation (3.38), whereas the dotted line corresponds to the eigenfrequency computed using the asymptotic formulae (4.9). In addition, 3D finite element computations for the same structure using COSMOS are included in this figure as circles, for comparison. Finally, we note that the stars on the y -axes of each graph in Fig. 4 represent a structure with three legs only, formally constructed for the case when $p = 0$. Again, COSMOS is used for the finite element computations. Specifically,

these values are

$$(4.11) \quad f_r^{(1)} \approx 7.30 \text{ [Hz]}, \quad f_r^{(2)} \approx 7.94 \text{ [Hz]}, \quad f_r^{(3)} \approx 6.61 \text{ [Hz]}.$$

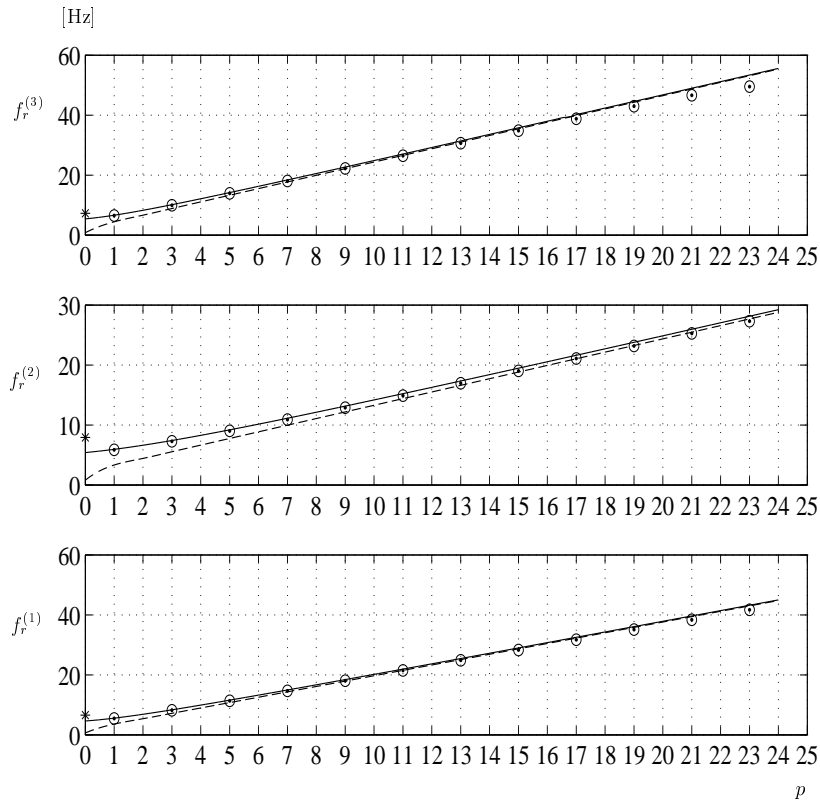


FIG. 4. Eigenfrequencies $f_r^{(j)}$ versus the parameter p , where $j = 1, 2, 3$ indicates the respective rotation about the x_j -axis: Solid lines denote the numerical solution of (3.38), dotted lines denote analytical asymptotic solution given in (4.9) and the circles are obtained by direct 3D finite element calculations.

We note that the star values are located above all the curves. At first, this may seem like a contradiction, however, the structure with three legs only is different than the structure with six legs with zero distance between the pairs. Since the three-leg structure is stiffer than the six-leg structure, the corresponding eigenfrequencies are larger. This issue is discussed in detail in the next section.

It is also important to underline that the difference between the eigenfrequencies corresponding to translational modes calculated asymptotically and those calculated numerically is significantly small. For instance, the difference between the maximum values of $f_t^{(j)}$ computed asymptotically and the maximum values

of $f_t^{(j)}$ computed numerically is less than $4 \cdot 10^{-2}\%$. Hence, in what follows, we will mainly be concerned with the rotational modes only.

It is clear that when p is small, that is, when the legs are sufficiently close to each other, asymptotic formulae do not coincide with the numerical solution. In fact, when $p = 1$, i.e. the distance between the nearest legs is 2 cm, the percentage difference between the values computed asymptotically and numerically for $f_r^{(1)}$, $f_r^{(2)}$ and $f_r^{(3)}$ is 33%, 44% and 35.5%, respectively. Moreover, when $p \rightarrow 0$, the difference is nearly 100% (see Fig. 5).

We emphasise the fact that the asymptotic formulae (4.9) are remarkably accurate for larger values of the parameter p as shown in Fig. 4 and Fig. 5. The formulae are also simple, and are useful in understanding the effect of different parameters. Moreover, in the case when the curves for different eigenfrequencies intersect each other (see Fig. 3), finite element computations and numerical solutions face unexpected difficulties due to the change of order of the eigenfrequencies and the structure of the eigenvectors. These problems do not occur with the asymptotic formulae. Finally, we note that it is possible to improve our asymptotic procedure by taking into account the fact that $\det \Phi_0(p) \neq 0$ for any $p > 0$, but $\det \Phi_0(0) = O(\varepsilon^\alpha)$, $\varepsilon \rightarrow 0$. We recall that this means that our particular structure is *weakly nondegenerate* for small p .

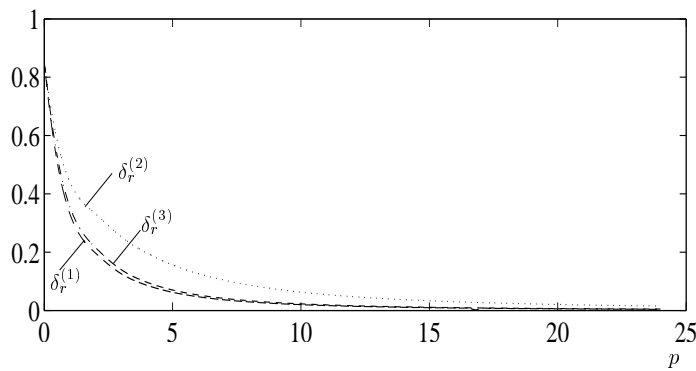


FIG. 5. Relative error between the asymptotic and numerical values of the eigenfrequencies $f_r^{(j)}$, $j = 1, 2, 3$ versus the parameter p .

Now, we discuss the difference between the eigenfrequencies of the 1D-3D multi-structure and the associated pile structure. It is possible to expect that this difference is bigger for small values of the parameter p since the effect of boundary layer fields near the legs may influence the results. It is interesting to observe that estimates (2.1) were proved in [3], under the assumption that the legs were sufficiently far from each other, however, our results show the contrary. For

values from $p = 1$ to $p = 13$ the eigenfrequencies differ by 1.5% to 2%, whereas for $p = 23$ this difference is 7.5%, 3% and 3.5% for the modes corresponding to rotations about the x_j -axis $j = 1, 2, 3$, respectively. The only explanation we have for this phenomena is associated with the effect of the structure of the boundary layer fields appearing near the edges of the parallelepiped.

We also note that Fig. 4 is consistent with the second inequality in (2.1), i.e. the circles corresponding to the eigenfrequencies obtained from the finite element computations all lie underneath the curve constructed for the associated pile structure. Moreover, this allows us to make a one-sided numerical estimate for the value of the parameter \mathcal{Q} which appears in the first inequality in (2.1):

$$(4.12) \quad \mathcal{Q} \geq \max\{Q_k\}, \quad Q_k = \frac{1}{\rho} (\omega_k^{-2} - \nu_k^{-2}), \quad k = 1, \dots, 6.$$

The graph for $Q_k(p)$ versus the parameter p is given in Fig. 6. Here the translational modes are omitted, since they are two orders of magnitude smaller than the rotational modes.

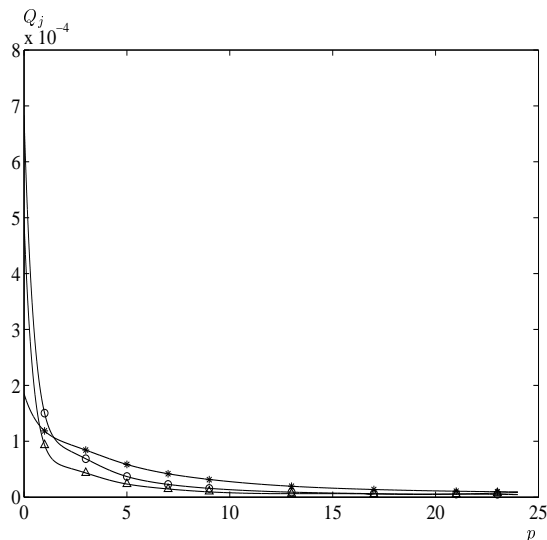


FIG. 6. One-sided numerical estimate for the parameter $\mathcal{Q} \geq Q_j$ (see (2.1)) versus the parameter p . The curves with triangles, stars and circles correspond to rotations about the x_j -axis ($j = 1, 2, 3$), respectively.

From Fig. 6 we also conclude that $\max\{Q_k(24)\}/\max\{Q_k(0)\}$, $k = 1, 2, 3$ is of order ε . Hence, one can expect the same estimate for the value of the ratio of the constant $\mathcal{Q}(24)/\mathcal{Q}(0)$. However, configuration for $p = 24$ is *nondegenerate* and for $p = 0$ is *weakly nondegenerate*. This means that \mathcal{Q} for the *nondegenerate*

structure should be much smaller than \mathcal{Q} for the *weakly nondegenerate* and for the *degenerate* structure with the same 3D body. Therefore, we have the possibility of proving accurate asymptotic estimates for *nondegenerate* structures, similar to the corresponding one, proved for *degenerate* structures in [3]. We recall that in [3] it was proved that $\mathcal{Q} \sim C \varepsilon^{-2}$, $\varepsilon \rightarrow 0$ for the particular *degenerate* structure discussed. This may seem like a contradiction since $Q_3(0) \approx 6.8 \cdot 10^{-4}$, however, the constant C depends on the elastic and geometrical parameters of the structure, and not on the thickness of the legs (the small parameter ε).

4.2. A particular example: A 1D-3D multi-structure with three legs

As mentioned in the previous section, we discuss the difference between a 1D-3D multi-structure with six legs (three adjacent pairs) and a 1D-3D multi-structure with three legs (see Fig. 7). Following the detailed discussions given before, the multi-structures are called *weakly nondegenerate* and *degenerate*, respectively.

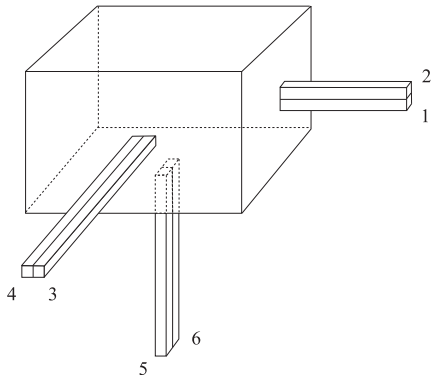


FIG. 7. A *degenerate* 1D-3D multi-structure with three legs.

For this particular choice of geometry formula (3.42) is still valid (since Sec. 3.2. deals with the description of general asymptotics) and therefore will be used to obtain asymptotic representations for the first six eigenfrequencies of the multi-structure.

The body Ω of dimensions a_1 , a_2 and a_3 is supported by three legs, with the following junction points and unit vectors defining their directions:

$$\mathbf{a}^{(1)} = \left(\frac{a_1}{2}, 0, -\frac{a_3}{2} \right)^\top, \quad \mathbf{a}^{(2)} = \left(0, \frac{a_2}{2}, -\frac{a_3}{2} \right)^\top, \quad \mathbf{a}^{(3)} = (0, 0, 0)^\top,$$

$$\boldsymbol{\mu}^{(1)} = (1, 0, 0), \quad \boldsymbol{\mu}^{(2)} = (0, 1, 0), \quad \boldsymbol{\mu}^{(3)} = (0, 0, 1).$$

Note that the matrices $\Lambda^{(j)}$ ($j = 1, 2, 3$) are those given in the previous section.

Again, all the legs are assumed to be homogeneous, isotropic and of the same elastic material. As before, we assume that the legs are of the same length l . Now the legs have the cross-section $b_1 \times b_2$, $b_2 > b_1$ (see Fig. 7). It is clear that in this particular problem the small parameter is $\varepsilon = b_2/l$.

After some elementary calculations it can be shown that the matrix $\mathbf{\Phi}_0$ can be written as $\mathbf{\Phi}_0 = El\mathbf{\Phi}_{0,0}$, where $\mathbf{\Phi}_{0,0} = (\phi_{k,l})$, and the nonzero elements are

$$\begin{aligned}\phi_{1,5} = \phi_{5,1} = -\phi_{2,4} = -\phi_{4,2} &= -\frac{a_3}{2}, \\ \phi_{1,1} = \phi_{2,2} = \phi_{3,3} = 1, \quad \phi_{4,4} = \phi_{5,5} &= \frac{a_3^2}{4}.\end{aligned}$$

The rank of the matrix $\mathbf{\Phi}_{0,0}$ is 3 and there are only three positive roots of equation (3.52):

$$(4.13) \quad q_0^{(4)} = q_0^{(5)} = q_0^{(6)} = El\Omega_0^{-1}\gamma, \quad \gamma = b_1/b_2 \in (0, 1).$$

These eigenfrequencies can be approximated by the following formula (multiplicity is caused by the symmetry of the multi-structure)

$$(4.14) \quad f_{4,5,6} \sim \frac{1}{2\pi} \sqrt{\frac{El\gamma}{\rho\Omega_0}} (b_2/l).$$

The last three solutions of Eq. (3.52) are equal to zero. To be able to find the first three eigenfrequencies it is necessary to consider Eq. (3.50) and use the representation of the matrix $\mathbf{\Phi}_1$. Using the facts that Eq. (3.50) has three roots of order $O(\varepsilon^2)$ for the case when $\varepsilon \neq 0$ and the matrices $\mathbf{\Phi}_0$, $\mathbf{\Phi}_1$ and $\mathbf{\Gamma}$ are symmetric, we find these roots as

$$(4.15) \quad f_k \sim \frac{1}{2\pi} \sqrt{\frac{12El\gamma\theta_k}{\rho\Omega_0}} (b_2/l)^2, \quad k = 1, 2, 3, \quad b_2 \rightarrow 0.$$

Here, we have used the following notations:

$$(4.16) \quad \begin{aligned}\theta_1 &= \frac{1}{a_1^2 + a_2^2} \left[\frac{l^2}{3} (1 + \gamma^2) + \frac{l^2\gamma^2\beta}{2(1+\nu)} + \frac{l}{2}a_1\gamma^2 + \frac{l}{2}a_2 + \frac{a_1^2}{4}\gamma^2 + \frac{a_2^2}{4} \right], \\ \theta_2 &= \frac{1}{a_1^2 + a_3^2} \left[\frac{l^2}{3} (1 + \gamma^2) + \frac{l^2\gamma^2\beta}{2(1+\nu)} + \frac{l}{2}a_1 + \frac{l}{2}a_3\gamma^2 + \frac{a_1^2}{4} + \frac{a_3^2}{4}\gamma^2 \right], \\ \theta_3 &= \frac{1}{a_2^2 + a_3^2} \left[\frac{l^2}{3} (1 + \gamma^2) + \frac{l^2\gamma^2\beta}{2(1+\nu)} + \frac{l}{2}a_2\gamma^2 + \frac{l}{2}a_3 + \frac{a_2^2}{4}\gamma^2 + \frac{a_3^2}{4} \right],\end{aligned}$$

$$(4.17) \quad \beta = \frac{1}{3} - \sum_{k=0}^{\infty} \frac{64\gamma}{\pi^5(2k+1)^5} \tanh \left[\frac{(2k+1)\pi}{2\gamma} \right].$$

It is relatively easy to check that $\beta \approx 0.141$ when $\gamma = 1$. This calculation requires the torsion potential, that is, the solution of a certain Neumann boundary value problem on the cross-section of a leg.

We refer to the same material properties as in the previous section. Hence, formulae (4.14) and (4.15) lead to

$$f_1 \approx 6.67 \text{ [Hz]}, \quad f_2 \approx 7.40 \text{ [Hz]}, \quad f_3 \approx 8.04 \text{ [Hz]}, \quad f_{4,5,6} \approx 39.49 \text{ [Hz]},$$

while the finite element computations performed by COSMOS give

$$f_1 \approx 6.61 \text{ [Hz]}, \quad f_2 \approx 7.30 \text{ [Hz]}, \quad f_3 \approx 7.94 \text{ [Hz]}, \quad f_{4,5,6} \approx 39.24 \text{ [Hz]}.$$

Hence, the accuracy of the asymptotic formulae is clear.

5. Concluding remarks and further work

The present paper is a continuation of our interest in problems posed for multi-structures, which has a wide range of practical applications.

Here, we gave an accurate formulation of an eigenvalue problem for a 1D-3D multi-structure and described general asymptotics for the skeleton. This led us to the interesting issue of degeneracy associated with a 1D-3D multi-structure and we defined so-called *weak nondegeneracy*. The different possibilities of configurations leading to *weak nondegeneracy* are endless (see, for example, Fig. 8). Hence, instead of analysing different configurations, we concentrated on a particular case and analysed this in detail. For this particular example, we constructed analytical asymptotic formulae for the first six eigenfrequencies, which makes it possible to analyse the behaviour of these frequencies with respect to all parameters of the structure. The accuracy of these formulae was also tested against numerical and finite element computations, which showed interesting and unexpected effects. We emphasise once more that the inaccuracies faced by numerical and finite element computations, for the case when some of the eigenfrequencies are close to each other, are absent in our asymptotic results. Remarkably, these inaccuracies occur in the regions in which the asymptotic formulae are most reliable. It is also interesting to note that the accuracy of the pile structure solution is high, even for small distances between the legs. We believe that these results are difficult to predict without a detailed analysis, such as that given in the present paper.

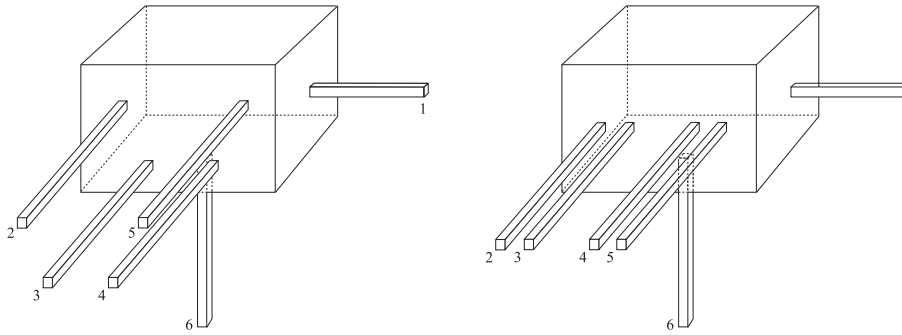


FIG. 8. A 1D-3D homogeneous multi-structure, illustrating a different type of *weak nondegeneracy*.

To establish a two-sided estimate for the finite-dimensional approximation to a 1D-3D multi-structure, it is important to know the value of the constant \mathcal{Q} in (2.1). However, it is difficult to find this constant rigorously. In fact, it is only possible to estimate it with respect to the small parameter associated with the multi-structure. Our calculations lead to the result that the value for the constant \mathcal{Q} is different for *degenerate* and *nondegenerate* multi-structures.

Future work is on the rigorous estimates of the constant discussed above. In addition to this we are also interested in analysing 1D-3D nonhomogeneous multi-structures, which have applications in damage mechanics.

Acknowledgments

This research project has been supported by a Marie Curie Transfer of Knowledge Fellowship of the European Community's Sixth Framework Programme under contract number MTKD-CT-2004-509809. Ö. Selsil would like to thank the Rzeszów University of Technology, Poland for their kind hospitality during his stay which was supported by the EU Marie Curie grant (ToK scheme), contract number. The authors are also grateful to Prof. A. B. Movchan for discussions.

Appendix A.

We denote the stiffness coefficients of the legs $\Pi_\varepsilon^{(j)}$ by $C_i^{(j)}$, $i = 1, 2, 3, 4$, $j = 1, \dots, K$, where

$$(A.1) \quad C_i^{(j)} = E \int_{g^{(j)}} y_i^{(j)2} dy_1^{(j)} dy_2^{(j)}, \quad i = 1, 2,$$

stand for the tranverse displacements,

$$(A.2) \quad C_3^{(j)} = E \operatorname{mes} (g^{(j)})$$

corresponds to the longitudinal displacement and

$$(A.3) \quad C_4^{(j)} = \frac{E}{2(1+\nu)} \int_{g^{(j)}} \|\nabla \varphi^{(j)} - y_2^{(j)} \mathbf{e}_1^{(j)} + y_1^{(j)} \mathbf{e}_2^{(j)}\|^2 dy_1^{(j)} dy_2^{(j)},$$

corresponds to the axial rotation. Here, $\varphi^{(j)}$ is the torsion potential (see, for example, [4]).

It is clear that

$$(A.4) \quad C_i^{(j)} = \varepsilon^4 C_{i,0}^{(j)}, \quad k = 1, 2, 4, \quad C_3^{(j)} = \varepsilon^2 C_{3,0}^{(j)},$$

where $C_{i,0}^{(j)}$, $i = 1, 2, 3, 4$, $j = 1, \dots, K$, do not depend on ε .

The functions $\hat{v}_i^{(j)}$, $i = 1, 2, 3, 4$, $j = 1, \dots, K$ satisfy the ordinary differential equations

$$(A.5) \quad \begin{aligned} \frac{d^4 \hat{v}_i^{(j)}}{dy_3^{(j)4}} (y_3^{(j)}) &= 0, & 0 < y_3^{(j)} < l^{(j)}, & \quad i = 1, 2, \\ \frac{d^2 \hat{v}_i^{(j)}}{dy_3^{(j)2}} (y_3^{(j)}) &= 0, & 0 < y_3^{(j)} < l^{(j)}, & \quad i = 3, 4. \end{aligned}$$

The transmission conditions at junction points $\mathbf{a}^{(j)}$, $j = 1, \dots, K$ are formulated as

$$(A.6) \quad \hat{v}_i^{(j)}(0) = \hat{\alpha}_i^{(j)} + (\hat{\boldsymbol{\beta}}^{(j)} \times \hat{\mathbf{a}}^{(j)})_i, \quad i = 1, 2, 3,$$

$$(A.7) \quad \hat{v}_4^{(j)}(0) = \hat{\beta}_3^{(j)}, \quad \frac{d\hat{v}_1^{(j)}}{dy_3^{(j)}}(0) = \hat{\beta}_2^{(j)}, \quad \frac{d\hat{v}_2^{(j)}}{dy_3^{(j)}}(0) = -\hat{\beta}_1^{(j)},$$

and the clamping conditions on S_ε lead to

$$(A.8) \quad \hat{v}_i^{(j)}(l^{(j)}) = 0, \quad i = 1, 2, 3, 4, \quad \frac{d\hat{v}_i^{(j)}}{dy_3^{(j)}}(l^{(j)}) = 0, \quad i = 1, 2.$$

The components of the forces and the moments, exerted by the legs $\Pi_\varepsilon^{(j)}$ on the body Ω , in local coordinates, can be written as (see (3.15))

$$(A.9) \quad \hat{\mathcal{F}}_i^{(j)} = -C_i^{(j)} \frac{d^3 \hat{v}_i^{(j)}(0)}{dy_3^{(j)3}}, \quad i = 1, 2, \quad \hat{\mathcal{F}}_3^{(j)} = C_3^{(j)} \frac{d\hat{v}_3^{(j)}(0)}{dy_3^{(j)}},$$

$$(A.10) \quad \hat{\mathcal{M}}_{3-i}^{(j)} = (-1)^{i+1} C_i^{(j)} \frac{d^2 \hat{v}_i^{(j)}(0)}{dy_3^{(j)2}}, \quad i = 1, 2, \quad \hat{\mathcal{M}}_3^{(j)} = C_4^{(j)} \frac{d\hat{v}_4^{(j)}(0)}{dy_3^{(j)}},$$

where $C_i^{(j)}$, $i = 1, 2, 3, 4$, $j = 1, \dots, K$ are positive stiffness coefficients and $\hat{v}_i^{(j)}$, $i = 1, 2, 3, 4$, $j = 1, \dots, K$ are given by

$$\begin{aligned}\hat{v}_1^{(j)}(y_3^{(j)}) &= \phi_I(y_3^{(j)}/l^{(j)})(\hat{\alpha}_1^{(j)} + (\hat{\boldsymbol{\beta}}^{(j)} \times \hat{\mathbf{a}}^{(j)})_1) + l^{(j)}\phi_{II}(y_3^{(j)}/l^{(j)})\hat{\beta}_2^{(j)}, \\ \hat{v}_2^{(j)}(y_3^{(j)}) &= \phi_I(y_3^{(j)}/l^{(j)})(\hat{\alpha}_2^{(j)} + (\hat{\boldsymbol{\beta}}^{(j)} \times \hat{\mathbf{a}}^{(j)})_2) - l^{(j)}\phi_{II}(y_3^{(j)}/l^{(j)})\hat{\beta}_1^{(j)}, \\ \hat{v}_3^{(j)}(y_3^{(j)}) &= (1 - y_3^{(j)}/l^{(j)})(\hat{\alpha}_3^{(j)} + (\hat{\boldsymbol{\beta}}^{(j)} \times \hat{\mathbf{a}}^{(j)})_3), \\ \hat{v}_4^{(j)}(y_3^{(j)}) &= (1 - y_3^{(j)}/l^{(j)})\hat{\beta}_3^{(j)},\end{aligned}$$

with

$$\phi_I(t) = (t-1)^2(2t+1), \quad \phi_{II}(t) = (t-1)^2t.$$

Hence, Eqs. (A.9) and (A.10) can be written explicitly as

$$\begin{aligned}\hat{\mathcal{F}}_1^{(j)} &= -C_1^{(j)} \left\{ 12 \left[\hat{\alpha}_1^{(j)} + (\hat{\boldsymbol{\beta}}^{(j)} \times \hat{\mathbf{a}}^{(j)})_1 \right] / l^{(j)3} + 6\hat{\beta}_2^{(j)} / l^{(j)2} \right\}, \\ \hat{\mathcal{F}}_2^{(j)} &= -C_2^{(j)} \left\{ 12 \left[\hat{\alpha}_2^{(j)} + (\hat{\boldsymbol{\beta}}^{(j)} \times \hat{\mathbf{a}}^{(j)})_2 \right] / l^{(j)3} - 6\hat{\beta}_1^{(j)} / l^{(j)2} \right\}, \\ \hat{\mathcal{F}}_3^{(j)} &= -C_3^{(j)} \left[\hat{\alpha}_3^{(j)} + (\hat{\boldsymbol{\beta}}^{(j)} \times \hat{\mathbf{a}}^{(j)})_3 \right] / l^{(j)}, \\ \hat{\mathcal{M}}_1^{(j)} &= C_2^{(j)} \left\{ 6 \left[\hat{\alpha}_2^{(j)} + (\hat{\boldsymbol{\beta}}^{(j)} \times \hat{\mathbf{a}}^{(j)})_2 \right] / l^{(j)2} - 4\hat{\beta}_1^{(j)} / l^{(j)} \right\}, \\ \hat{\mathcal{M}}_2^{(j)} &= C_1^{(j)} \left\{ -6 \left[\hat{\alpha}_1^{(j)} + (\hat{\boldsymbol{\beta}}^{(j)} \times \hat{\mathbf{a}}^{(j)})_1 \right] / l^{(j)2} - 4\hat{\beta}_2^{(j)} / l^{(j)} \right\}, \\ \hat{\mathcal{M}}_3^{(j)} &= -C_4^{(j)} \hat{\beta}_3^{(j)} / l^{(j)}.\end{aligned}\tag{A.11}$$

Appendix B.

We note that $\mathbf{R}^{(j)}, \mathbf{T}^{(j)}$, $j = 1, \dots, K$ are diagonal matrices. In addition, the relationship $(\mathbf{A}^{(j)})^\top = -\mathbf{A}^{(j)}$ holds true for the matrix $\mathbf{A}^{(j)}$ (see (3.21)). Hence, it is straightforward to show that

$$(\boldsymbol{\Phi}_{1,1})^\top = \boldsymbol{\Phi}_{1,1}, \quad \boldsymbol{\Phi}_{2,1} = (\boldsymbol{\Phi}_{1,2})^\top, \quad (\boldsymbol{\Phi}_{2,2})^\top = \boldsymbol{\Phi}_{2,2}.$$

Therefore, the matrix $\boldsymbol{\Phi}$ is symmetric.

To prove that the matrix $\boldsymbol{\Phi}$ is positive definite, we consider the following expression

$$(B.1) \quad e = \mathcal{F} \cdot \boldsymbol{\alpha} + \mathcal{M} \cdot \boldsymbol{\beta},$$

which is equivalent to (see (3.23) and (3.35))

$$(B.2) \quad e = \Phi \boldsymbol{\theta} \cdot \boldsymbol{\theta}.$$

In addition, using the balance relations (3.14) we can write

$$(B.3) \quad \begin{aligned} e &= \mathcal{F} \cdot \boldsymbol{\alpha} + \mathcal{M} \cdot \boldsymbol{\beta} = - \sum_{j=1}^K \mathcal{F}^{(j)} \cdot \boldsymbol{\alpha} - \sum_{j=1}^K (\mathcal{M}^{(j)} + \mathbf{a}^{(j)} \times \mathcal{F}) \cdot \boldsymbol{\beta} \\ &= - \sum_{j=1}^K \hat{\mathcal{F}}^{(j)} \cdot (\hat{\boldsymbol{\alpha}}^{(j)} - \hat{\mathbf{a}}^{(j)} \times \hat{\boldsymbol{\beta}}^{(j)}) - \sum_{j=1}^K \hat{\mathcal{M}}^{(j)} \cdot \hat{\boldsymbol{\beta}}^{(j)}. \end{aligned}$$

Now, using the formulae (A.9) and (A.10), Eq. (B.3) can be rewritten as

$$(B.4) \quad e = \sum_{j=1}^K \sum_{i=1}^2 \left\{ C_i^{(j)} \left[\frac{d^3 \hat{v}_i^{(j)}}{dy_3^{(j)3}} \Big|_{y_3^{(j)}=0} \hat{v}_i^{(j)} \Big|_{y_3^{(j)}=0} - \frac{d^2 \hat{v}_i^{(j)}}{dy_3^{(j)2}} \Big|_{y_3^{(j)}=0} \frac{d \hat{v}_i^{(j)}}{dy_3^{(j)}} \Big|_{y_3^{(j)}=0} \right] - C_{i+2}^{(j)} \frac{d \hat{v}_{i+2}^{(j)}}{dy_3^{(j)}} \Big|_{y_3^{(j)}=0} v_{i+2}^{(j)} \Big|_{y_3^{(j)}=0} \right\}.$$

It can be shown that e can be also represented as

$$(B.5) \quad e = \sum_{j=1}^K \int_0^{l^{(j)}} \sum_{i=1}^2 \left[C_i^{(j)} \left(\frac{d^2 \hat{v}_i^{(j)}}{dy_3^{(j)2}} \right)^2 + C_{i+2}^{(j)} \left(\frac{d \hat{v}_{i+2}^{(j)}}{dy_3^{(j)}} \right)^2 \right] dy_3^{(j)}.$$

To be able to show the equivalence of (B.4) and (B.5), one has to use integration by parts for the right-hand side of equation (B.5) and employ the differential equations (see (A.5)) and boundary conditions on S_ε posed for the functions $\hat{v}_i^{(j)}$, $i = 1, 2, 3, 4$, $j = 1, \dots, K$ (see (A.8)).

It follows that $e > 0$. Hence, for an arbitrary vector $\boldsymbol{\theta} \neq \mathbf{0}$ (see (B.2)), $\Phi > 0$, provided that at least one of the functions $\hat{v}_i^{(j)}$ is not identically zero. This completes the proof.

References

1. V.G. MAZ'YA, S.A. NAZAROV, B.A. PLAMENEVSKII, *Asymptotische Theorie elliptischer Randwertaufgaben in singulär gestörten Gebieten*, Akademie-Verlag Berlin, B.1, 1991; B.2, 1992.
2. P.G. CIARLET, *Mathematical elasticity, Vol. II: Theory of plates*, North-Holland, Amsterdam 1997.

3. V.A. KOZLOV, V.G. MAZ'YA, A.B. MOVCHAN, *Asymptotic analysis of fields in multi-structures*, Oxford University Press, 1999.
4. V.A. KOZLOV, V.G. MAZ'YA, A.B. MOVCHAN, *Asymptotic analysis of a mixed boundary value problem in a multi-structure*, *Asymptotic Analysis*, **8**, 105–143, 1994.
5. V.A. KOZLOV, V.G. MAZ'YA, A.B. MOVCHAN, *Asymptotic representation of elastic fields in a multi-structure*, *Asymptotic Analysis*, **11**, 343–415, 1995.
6. V.A. KOZLOV, V.G. MAZ'YA, A.B. MOVCHAN, *Fields in nondegenerate 3D-1D elastic multi-structures*, LiTH-MAT-R-96-14, Preprint, Linköping University, 1996.
7. A.G. ASLANYAN, A.B. MOVCHAN, O. SELSIL, *Vibrations of multi-structures including elastic shells: Asymptotic analysis*, *Euro. J. of Applied Mathematics*, **11**, 109–128, 2002.
8. A.G. ASLANYAN, A.B. MOVCHAN, O. SELSIL, *Estimates for the low eigenfrequencies of a multi-structure including an elastic shell*, *Euro. J. of Applied Mathematics*, **14**, 313–342, 2003.
9. A.G. ASLANYAN, A.B. MOVCHAN, O. SELSIL, *Asymptotics for the first six eigenfrequencies of a 1D-3D multi-structure*, *Proceedings of IUTAM international symposium on Asymptotics, Singularities and Homogenisation in Problems of Mechanics*, Liverpool, UK, 221–228, 2003.
10. S.O. ASPLUND, *Structural mechanics: Classical and matrix methods*, Prentice Hall, Englewood Cliffs, NJ 1966.
11. Matlab, 6.5 The language of technical computing, 2002.
12. COSMOS/M.20, *A complete finite element analysis system*, Structural Research & Analysis Corp., 1997.

Received March 29, 2005.
